

# The mechanics and fluctuation spectrum of active gels

Alex J. Levine

*Department of Chemistry & Biochemistry  
and*

*The California Nanosystems Institute*

*University of California, Los Angeles, CA 90095, USA*

F.C. MacKintosh

*Department of Physics and Astronomy, Vrije Universiteit, Amsterdam, The Netherlands.*

(Dated: September 15, 2008)

Recent experiments on molecular motor driven *in vitro* F-actin networks have found anomalously large strain fluctuations at low frequency. In addition, the shear modulus of these active networks becomes as much as one hundred times larger than that of the same system in equilibrium. We develop a two-fluid model of a low-density semiflexible network driven by molecular motors to explore these effects and show that, relying on only simple assumptions regarding the motor activity in the system we can quantitatively understand both the low-frequency fluctuation enhancement and the non-equilibrium stiffening of the network. These results have implications for the interpretation of microrheology in such active networks including the cytoskeleton of living cells. In addition, they may form the basis for theoretical studies of biomimetic non-equilibrium gels whose mechanical properties are tunable through the control of their non-equilibrium steady-state.

## I. INTRODUCTION

Understanding the dynamics and mechanics of the cytoskeleton of eukaryotic cells is a forefront problem in biological physics and soft condensed matter. The system is one of daunting complexity, being both chemically heterogeneous and varying spatially over length scales ranging from tens of microns down to nanometers. But, to a first approximation it may be described as a cross-linked semiflexible filament network that pervades a large fraction of the cellular interior. One of the principal components of this network is filamentous actin or F-actin, a double stranded helical aggregate of globular or G-actin [1–3]. In living cells the actin filaments are typically cross-linked by a plethora of actin binding proteins that link actin filaments. In addition to F-actin, the cytoplasm contains other protein biopolymers, including much more rigid microtubules and more flexible intermediate filaments. The dynamics of this network is correspondingly complex, having a variety of active processes operating on different time scales, as well as the ever-present thermal or Brownian motion [4–12]. On very short time scales of order milliseconds, the cytoplasm appears as an equilibrium material, with similar dynamics to *in vitro* gels in equilibrium [13, 14], while on long time scales of order minutes, significant remodeling of the cytoskeleton occurs. Such remodeling is largely directed in nature, and involves, e.g., the polymerization/depolymerization of polar filaments. On intermediate time scales, however, active processes generate motion on a scale at least comparable to thermal motion [13, 15]. Although molecular motors are implicated here, the resulting motion is largely non-directed and can appear Brownian.

In order to develop a quantitative understanding of the complex dynamics of the cytoskeleton, there has

been much effort in developing equilibrium *in vitro* networks of reduced biochemical complexity [16–29]. Several simplified model systems have also been developed to address the non-equilibrium behavior due to molecular motors [30–33]. Here, we describe a theoretical model for active gels that is motivated by the recent experiments of Mizuno et al., [32] on a permanently cross-linked F-actin network driven by myosin-II molecular motors. These experiments examined the effect of driving a (solid) network out of equilibrium through the action of ATP-consuming molecular motors that apply stochastic strains to it. They find two dramatic results arising from the motor activity in the actin network: (i) motor activity leads to a significant stiffening of the network, with the linear elastic shear modulus increasing by as much as a factor of 100; and (ii) motor activity generates a significant increase in the low-frequency strain fluctuations of the network. Interestingly, even with motor activity in the network, the fluctuation spectrum of tracer particles embedded in the network is consistent with the expected thermal fluctuations at high frequencies.

These results present an interesting theoretical challenge, and have implications for both understanding the mechanics of living cells and for creating biomimetic materials with reversibly tunable elastic properties. It should be noted that this out-of-equilibrium system is distinct from previously studied systems of actively driven particulate solutions [35–38] in that the present system has a well-defined strain field and can support the stresses that develop due to the motors; the active force generating elements cannot create persistent flows in the solid material. We show below that one can quantitatively understand the motor-driven stiffening of the network at a mean-field level through the interaction of the inherent elastic nonlinearity of F-actin under tension [34] with motor forces. We also present a calculation

of the strain fluctuation spectrum of the driven material in the limit of low motor concentration. Understanding the detailed form of this fluctuation spectrum has wide-ranging implications for the quantitative interpretation of microrheology in living cells.

Microrheology [18, 39–43] has made possible a number of rheological measurements that would otherwise be impractical because of either the small size or fragility of the sample, or its inaccessibility preventing a direct mechanical coupling. One particularly important class of systems that benefit from microrheological studies are living cells [13, 15, 44–50]. The interpretation of tracer fluctuations in terms of rheology/mechanics relies generally on the assumption of thermal equilibrium. The presence of motor forces in the cytoskeleton invalidates this theoretical framework, and new theoretical approaches [13, 51–56] are clearly needed.

The remainder of this article is organized as follows. We discuss the two-fluid model for the mechanics of gels in section II A. We then describe the motor-induced forces driving this network in section II B, and then calculate the predicted tracer fluctuation spectrum in section III A. We then turn to the question of the stiffening of the network in response to endogenous motor activity in section III B, before presenting a summary and discussion of ongoing and future work in section IV. In order to improve readability, we relegate much of the calculational details of this work to appendices A–C.

## II. THE MODEL

### A. The network

To describe mechanics of the network and the background (aqueous) solvent we use the well-known two-fluid model first introduced by de Gennes and Broachard [57–59] and subsequently broadly used to model the dynamics of polymer gels [60–63]. More recently, this model has been used to understand the semiflexible biopolymer gels, such as those of the cytoskeleton [18, 56, 64, 65]. This model describes a gel in terms of two dynamical fields: the displacement field  $\mathbf{u}$  of the network and the velocity field  $\mathbf{v}$  of the permeating solvent. The dynamics of this model are given by

$$\rho \frac{\partial \mathbf{v}}{\partial t} = \eta \nabla^2 \mathbf{v} - \nabla p + \Gamma \left( \frac{\partial \mathbf{u}}{\partial t} - \mathbf{v} \right) + \mathbf{f}^{(v)} \quad (1)$$

$$\rho_N \frac{\partial^2 \mathbf{u}}{\partial t^2} = \mu \nabla^2 \mathbf{u} + (\mu + \lambda) \nabla (\nabla \cdot \mathbf{u}) - \Gamma \left( \frac{\partial \mathbf{u}}{\partial t} - \mathbf{v} \right) + \mathbf{f}^{(u)}. \quad (2)$$

In Eq. (1) we have assumed low-Reynolds number dynamics and we thus use the linearized Navier-Stokes equation. In that equation,  $\rho$  and  $\eta$  are the solvent density and viscosity. The mechanics of the gel as described by the continuum model given in Eq. (3) can be written in

terms of two Lamé coefficients necessary for an isotropic solid [66]. This continuum model is a valid description of the system’s dynamics on sufficiently large length scales. Determining this length scale is somewhat subtle due to the fact that the thermal persistence length of the semiflexible actin filaments is on the order of  $20\mu\text{m}$ , which is generally an order of magnitude larger than the mesh size of the network  $\xi$  – see Fig.(1). We discuss in more detail the limits of applicability of the two-fluid model in section IV.

The two force densities  $\mathbf{f}^{(v)}$  and  $\mathbf{f}^{(u)}$  represent any applied forces to the solvent and network respectively. In particular, the molecular motors will act on the network through  $\mathbf{f}^{(u)}$ . In writing Eq. (3), we have neglected the inertia of the network in comparison to that of the fluid. This is reasonable since the biopolymer network has a density similar to that of water, but typically has a volume fraction  $\phi$  on the order of  $10^{-3}$  so that its mass density is negligible in comparison to that of the solvent.

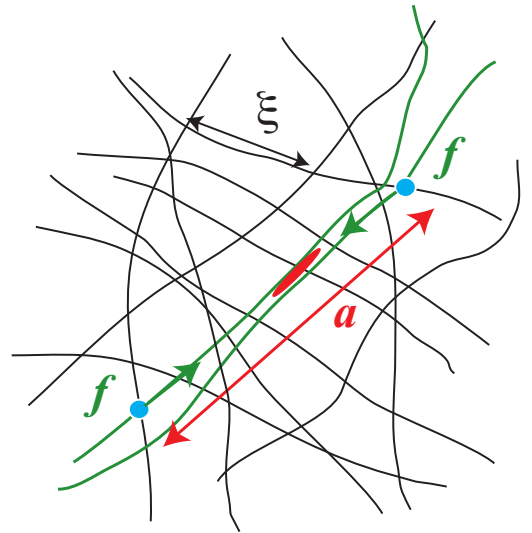


FIG. 1: (color online) Schematic diagram of a molecular motor acting on the network. The motor (red) slides the two filaments to which it is bound past each other. This action generates tensile stresses along the two active filaments (green) generating a pair of equal and opposite forces (green arrows) separated by a distance  $a > \xi$ .

These equations are supplemented by the requirement of volume conservation in the two-fluid medium,

$$\nabla \cdot \left[ \phi \frac{\partial \mathbf{u}}{\partial t} + (1 - \phi) \mathbf{v} \right] = 0. \quad (3)$$

Another consequence of our assumption that the network occupies a vanishingly small fraction of the volume,  $\phi \ll 1$ , is that Eq. (3) may be approximated by  $\nabla \cdot \mathbf{v} = 0$ , which expresses simply the incompressibility of the background solvent. The network, however, remains compressible, although its mass density can safely be ignored.

Finally, it is important to point out that the mechanics of the gel and the permeating solvent are coupled by the terms proportional to  $\Gamma$  in Eqs. (1) and (3). Due to Galilean invariance, this coupling must be a function of only the local difference in network and fluid velocities. We assume that nonlinear terms in the velocity difference are subdominant at least at the low velocities relevant to the biological system. This assumption results in a Darcy relation between the permeation velocity  $\dot{\mathbf{u}} - \mathbf{v}$  and the stress on the fluid parameterized by a single constant  $\Gamma$ . As discussed elsewhere [18, 64, 65], we estimate this constant as follows: the drag force per unit volume on the network for a given permeation velocity  $\Delta\mathbf{v}$  is, according to Eq. (3)  $\Gamma\Delta\mathbf{v}$ . However, the drag force on a single filament at the scale of the mesh size  $\xi$  is proportional to  $\eta\xi\Delta\mathbf{v}$  so the force density is  $\sim\eta\Delta\mathbf{v}\xi^{-2}$ , implying that  $\Gamma\sim\eta/\xi^2$ . This drag is the force density required to drive the fluid of viscosity  $\eta$  through network pores of characteristic area  $\xi^2$ .

We wish to determine the response of the combined network and fluid to an applied set of force densities  $\mathbf{f}^{(v)}(\mathbf{x}, t)$ ,  $\mathbf{f}^{(u)}(\mathbf{x}, t)$  acting on the fluid and network respectively. Due to the translational invariance of the system, it is convenient to solve this problem in Fourier space where we define

$$\mathbf{u}(\mathbf{x}, t) = \int \frac{d^3\mathbf{k}}{(2\pi)^3} e^{i(\mathbf{k}\cdot\mathbf{x} - \omega t)} \mathbf{u}(\mathbf{k}, \omega), \quad (4)$$

and an analogous equation for the fluid velocity field  $\mathbf{v}(\mathbf{x}, t)$ . In the Fourier representation Eqs. (1) and (3) become a set of six algebraic equations for  $\mathbf{u}(\mathbf{q}, \omega)$  and  $\mathbf{v}(\mathbf{q}, \omega)$  of the form

$$\mathcal{M}_{\alpha\beta}(\mathbf{q}, \omega) \mathcal{U}_\beta(\mathbf{q}, \omega) = \mathcal{F}_\alpha(\mathbf{q}, \omega), \quad (5)$$

where we have introduced a six-component column vector of displacements and velocities  $\mathcal{U}_\alpha(\mathbf{q}, \omega) = [\mathbf{u}(\mathbf{q}, \omega), \mathbf{v}(\mathbf{q}, \omega)]^T$  and an analogous six component column vector of the applied force densities  $\mathcal{F}_\alpha(\mathbf{q}, \omega) = [\mathbf{f}^{(u)}(\mathbf{q}, \omega), \mathbf{f}^{(v)}(\mathbf{q}, \omega)]^T$ . The  $6 \times 6$  matrix is shown in appendix A. The Greens function of the system in the Fourier domain is now clearly the inverse of the matrix  $\mathcal{M}_{\alpha\beta}(\mathbf{q}, \omega)$ . The calculation of the inverse of this object is greatly simplified by rewriting the above in terms of the transverse and longitudinal components of the fields  $\mathbf{u}$ ,  $\mathbf{v}$ . These components are generated by the action of their corresponding projection operators defined for an arbitrary vector field  $\mathbf{w}$  by

$$w_i^T(\mathbf{k}, \omega) = \mathcal{P}_{ij}^T(\mathbf{k}) w_j(\mathbf{k}, \omega) \quad (6)$$

$$w_j^L(\mathbf{k}, \omega) = \mathcal{P}_{ij}^L(\mathbf{k}) w_j(\mathbf{k}, \omega), \quad (7)$$

where  $\mathcal{P}_{ij}^T = \delta_{ij} - \hat{k}_i \hat{k}_j$  and  $\mathcal{P}_{ij}^L = \hat{k}_i \hat{k}_j$  are respectively the transverse and longitudinal projection operators. Working in these basis we invert Eq. (5) to determine the response of the system  $\mathcal{U}_\beta(\mathbf{q}, \omega)$  to force densities  $\mathcal{F}_\beta(\mathbf{q}, \omega)$  acting on both the fluid and the network. In the matrix inversion process care must be taken in order to allow

for a longitudinal part of the velocity field that is decoupled from the both the strain field and the transverse part of the fluid velocity field. Failure to do so renders  $\mathcal{M}_{\alpha\beta}(\mathbf{q}, \omega)$  singular; the inclusion of a (fictitious) longitudinal part of the fluid velocity field remedies this problem, while the decoupling of this field from the other dynamical variables allows for the restoration of fluid incompressibility simply by not driving this longitudinal part, i.e. setting  $\mathcal{P}_{ij}^L \mathbf{f}_j^{(v)}(\mathbf{q}, \omega) = 0$ . Performing this inversion we find:

$$u_i^L(\mathbf{k}, \omega) = \frac{\mathcal{P}_{ij}^L(\mathbf{k}) f_j^{(u)}}{-i\omega\Gamma + Bk^2} \quad (8)$$

$$u_i^T(\mathbf{k}, \omega) = \frac{\Delta(\mathbf{k}, \omega) \mathcal{P}_{ij}^T(\mathbf{k}) f_j^{(u)} + \Gamma \mathcal{P}_{ij}^T(\mathbf{k}) f_j^{(v)}}{\Delta(\mathbf{k}, \omega) \Phi(\mathbf{k}, \omega) + i\Gamma\omega^2} \quad (9)$$

$$v_i^T(\mathbf{k}, \omega) = \frac{-i\Gamma\omega \mathcal{P}_{ij}^T(\mathbf{k}) f_j^{(u)} + \Phi(\mathbf{k}, \omega) \mathcal{P}_{ij}^T(\mathbf{k}) f_j^{(v)}}{\Delta(\mathbf{k}, \omega) \Phi(\mathbf{k}, \omega) + i\Gamma\omega^2}, \quad (10)$$

where  $\Phi(\mathbf{k}, \omega) = -i\omega\Gamma + \mu k^2$ ,  $\Delta(\mathbf{k}, \omega) = -i\omega\rho + \eta k^2 + \Gamma$ , and  $B = 2\mu + \lambda$ . We will refer to  $B$  as the longitudinal modulus of the system. The rationale for this choice will be made clear below.

We now compute the response of the system to a point force applied to the network  $f_i^{(u)}(\mathbf{x}, t) = f_i \delta(\mathbf{x}) e^{-i\omega_0 t}$ . Since microrheological measurements are in actuality strain measurements of the network, we focus on the strain response of the network  $\mathbf{u}(\mathbf{x}, t)$ . Given the solutions in the Fourier domain for the longitudinal and transverse parts of the strain field given by Eqs. (8) and (9), the remaining computation involves only integrals over the wavevector using  $\mathbf{f}^{(u)}(\mathbf{q}, \omega) = \mathbf{f} \delta(\omega - \omega_0)$ ,  $\mathbf{f}^{(v)}(\mathbf{q}, \omega) = 0$ .

It is convenient to determine the longitudinal and transverse parts of the network strain response separately and then combine these results. The physics underlying this decomposition is that the two-fluid model has five hydrodynamic modes, i.e., modes whose relaxation rate vanishes in the long wavelength limit [67, 68]. Of these, four modes are propagating transverse oscillations of the combined network and solvent with a dispersion relation of the form  $\omega_k = \pm ck$ . The fifth mode is longitudinal and represents an overdamped network density mode in which the solvent does not participate. The dispersion relation of this mode has the form  $\omega_k = -iDk^2$ , giving the diffusive relaxation of network density. Thus, the structure of the propagator or Greens function corresponding to the response in the transverse and longitudinal channels differs and the calculation naturally decomposes into two independent parts.

We begin with the longitudinal response function. As shown in Appendix B, the longitudinal part of the response function, defined by

$$u_i(\mathbf{x}, \omega) = \mathcal{L}_{ij}(\mathbf{x}, \omega) f_j^{(u)}(\omega) \quad (11)$$

gives the amplitude of the strain response of the network (due to only the longitudinal channel) at a point  $\mathbf{x}$  due to

a force applied at the origin and having a sinusoidal temporal dependence  $e^{-i\omega t}$ . This function encodes the strain response of the network due to longitudinal or network-density changing deformations. The complex response tensor at finite frequency can be written as

$$\mathcal{L}_{ij}(\mathbf{x}, \omega) = \frac{1}{4\pi Br} \left[ t_1 \left( \frac{r}{\ell(\omega)} \right) \delta_{ij} + t_2 \left( \frac{r}{\ell(\omega)} \right) \hat{x}_i \hat{x}_j \right], \quad (12)$$

where we have defined the functions

$$t_1(x) = \frac{i}{x^2} [1 - e^{-\kappa x} (1 + \kappa x)] \quad (13)$$

$$t_2(x) = -\frac{3i}{x^2} \left[ 1 - \left( 1 + i\kappa^* x + \frac{1}{3} i x^2 \right) e^{-\kappa x} \right], \quad (14)$$

with

$$\kappa = \frac{1 - i}{\sqrt{2}}. \quad (15)$$

We have also introduced a frequency-dependent, dimensionless distance given by  $x = r/\ell(\omega)$  where we have defined the longitudinal penetration depth to be

$$\ell(\omega) = \sqrt{\frac{B(\omega)}{\Gamma\omega}}. \quad (16)$$

Here we write  $B$  as a function of frequency in anticipation of our consideration of a *viscoelastic* network.

This length scale determines the distance over which the longitudinal or density mode propagates outward into the two-fluid medium around a point force. As the driving frequency of the oscillating point force increases, the penetration depth of the network density variation decreases in a manner reminiscent of diffusive scaling. The underlying mechanics of this effect is simple. The network retains a longitudinal mode while the background solvent does not. Thus, longitudinal network deformation cannot be accompanied by corresponding deformations of the fluid so that the density mode of the network experiences a simple dissipative force density of the form  $\Gamma\omega\mathbf{u}$ . This is effectively just local Darcy drag. At high frequencies the Darcy drag is large so that the decay mode decays (exponentially) rapidly in space. As the frequency approaches zero, the compressible network decouples from the incompressible solvent so that the density mode decays as a power-law away from the point of force application.

To estimate a typical longitudinal penetration depth for experiments such as those in Ref. [32], we assume that the mesh-size on the order of  $10^2$ – $10^3$  nm and that the longitudinal modulus  $B$  has a roughly frequency-independent value on the order of  $10$ – $10^2$  Pa, then the penetration length  $\ell(\omega)$  for the longitudinal mode is of order  $10\mu\text{m}/\sqrt{\omega \cdot \text{s}}$ . On length scales below this, the response of the network can differ significantly from that of an incompressible material.

It remains to compute the contribution to the response function coming from the transverse modes of the system.

Using Eq. (9), neglecting the effects of the fluid's inertia, and making a simplification by restricting our consideration of the dynamics to length scales long compared to the mesh size (where this continuum model should be applicable), the transverse response in real space can be written in a simple form:

$$\mathcal{T}_{ij}(\mathbf{x}, \omega) = \frac{1}{8\pi|\mathbf{x}|(\mu - i\omega\eta)} [\delta_{ij} + \hat{x}_i \hat{x}_j]. \quad (17)$$

This response function is identical to that of transverse response of a viscoelastic isotropic continuum having a complex, frequency-dependent shear modulus  $G(\omega) = \mu - i\omega\eta$ . This is expected since in this inertia free, long wavelength limit the network and the fluid move in unison; even for a perfectly elastic network ( $\mu$  real and frequency independent) the composite material can be thought of as having a complex shear modulus.

Finally, we combine the longitudinal and transverse parts of the response tensor  $\alpha_{ij} = \mathcal{L}_{ij} + \mathcal{T}_{ij}$  to form the Greens function of the system. The total Greens tensor can be written as the sum of a parallel  $\alpha_{\parallel}$  and a perpendicular  $\alpha_{\perp}$  part so that

$$\alpha_{ij} = \alpha_{\parallel}(r, \omega) \hat{x}_i \hat{x}_j + \alpha_{\perp}(r, \omega) (\delta_{ij} - \hat{x}_i \hat{x}_j), \quad (18)$$

where  $r = |\mathbf{x}|$  and  $\hat{x} = \mathbf{r}/|\mathbf{r}|$  is a unit vector directed from the point of force application at the origin to the point where the strain field is evaluated at  $\mathbf{r}$ . Thus, the motion along the line connecting these two points is given by

$$\alpha_{\parallel}(r, \omega) = \frac{1}{4\pi r G(\omega)} \left[ 1 + \frac{G(\omega)}{B(\omega)} \chi_{\parallel} \left( \frac{r}{\ell(\omega)} \right) \right], \quad (19)$$

while the motion perpendicular to this line is given by

$$\alpha_{\perp}(r, \omega) = \frac{1}{8\pi r G(\omega)} \left[ 1 + \frac{G(\omega)}{B(\omega)} \chi_{\perp} \left( \frac{r}{\ell(\omega)} \right) \right]. \quad (20)$$

The two functions  $\chi_{\parallel}, \chi_{\perp}$  parameterize the effect of the longitudinal mode of the system in a spatial- and frequency-dependent manner. These functions are given by [56]

$$\chi_{\perp}(x) = \frac{2i}{x^2} [1 - (1 + \kappa x) e^{-\kappa x}] \quad (21)$$

$$\chi_{\parallel}(x) = e^{-\kappa x} - \chi_{\perp}(x). \quad (22)$$

As described below, the molecular motors generate pairs of anti-parallel forces and zero torque in the network. In Fig. 3 we plot the displacement field around such a pair of forces in the plane containing both of these forces. The pair of anti-parallel forces (red arrows) can generate significant local changes in network density. The length scale over which the density variation extends away from the distributed force dipole is controlled by the longitudinal penetration depth and is thus frequency dependent. In Fig. 4 we show the network density variation in the plane of the two forces making up

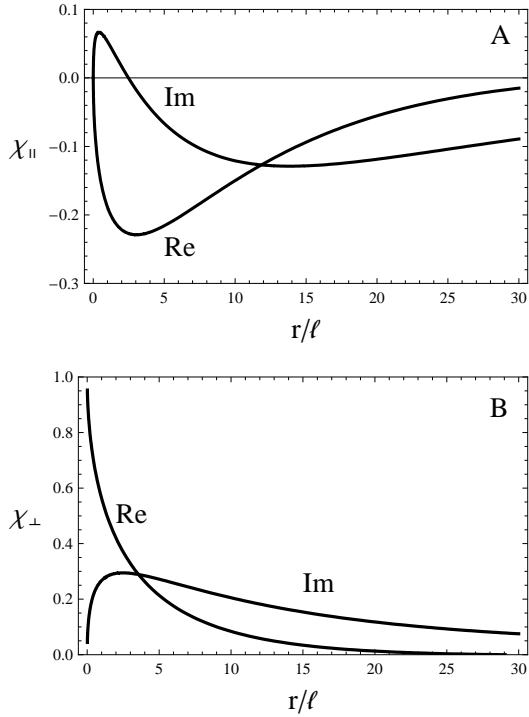


FIG. 2: The functions  $\chi_{\perp}(r/\ell)$  and  $\chi_{\parallel}(r/\ell)$  are plotted here as a function of the dimensionless length  $r/\ell$ . These functions, defined in Eqs. (21), (22) parameterize the spatial extent of the effect of the longitudinal mode of the network at a given frequency. The frequency-dependence of these results enters through the longitudinal penetration depth  $\ell(\omega)$  and has diffusive scaling as expected from the decay rate of the longitudinal mode.

a distributed dipole at frequencies of 0.1Hz and  $10^4$ Hz. The figure is axially symmetric about the line connecting these two force centers. From these figures it is clear that there are two lobes of increased network density centered at the midpoint between the two applied forces and extending preferentially in the plane normal to the line connecting the two force centers. There are two similar lobes of network rarefaction on either side of the force pair and extending outward along the line of centers of these two forces. The spatial extent of these lobes is simply controlled by the longitudinal penetration depth given in Eq. (16).

### B. The motors

We are interested in determining the fluctuation spectrum of the strain field in the active, or motor-driven gel. This fluctuation spectrum is typically discussed in microrheology in terms of the power spectrum of the strain fluctuations evaluated at one point in the material. This power spectrum takes the form  $\langle |\mathbf{u}(\omega)|^2 \rangle_M$ , where we have evaluated the strain field at the origin. The point of evaluation is irrelevant in light of the trans-

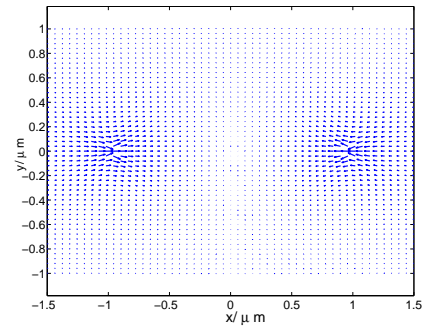


FIG. 3: (color online) The amplitude of the temporally oscillating vector field in the plane containing a pair of anti-parallel forces acting at  $\pm 1 \mu\text{m} \hat{x}$ . The viscosity of the solvent is taken to be that of water and the frequency of the sinusoidal time-dependence of the force pair is 0.1Hz. Distances in the figure are measured in microns.

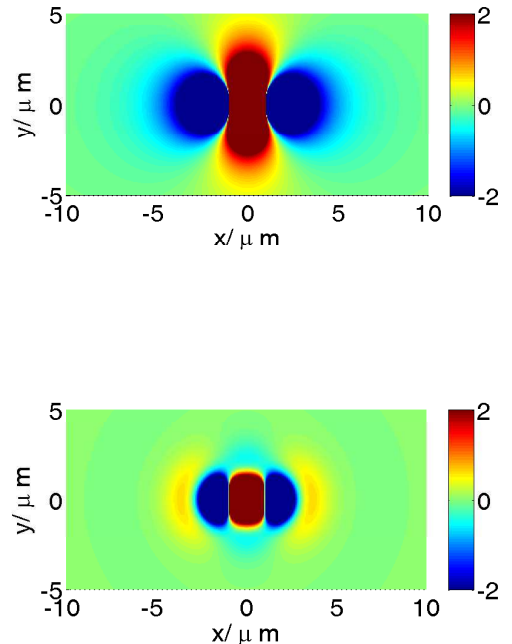


FIG. 4: (color online) a) A color map of the network compression field around a pair of anti-parallel forces placed symmetrically around the origin and along the  $x$ -axis. All distances are measured in microns; the color map shows the dimensionless fractional change in network density:  $\delta\rho_{\text{net}}/\rho_{\text{net}} = -\nabla \cdot \mathbf{u}$ . The longitudinal modulus is 300Pa and mesh size  $\xi = 300\text{nm}$ . The frequency of the sinusoidally varying force is 0.1Hz. In b) we plot the same quantities for the same network but with a frequency of  $10^4$ Hz. In both cases the force centers are placed on the  $\hat{x}$  axis at  $\pm 1 \mu\text{m}$ .

lational invariance of the system; we suppress the spatial variable here and in the following. The angled brackets are typically used to denote an average over an equilibrium ensemble of thermally fluctuating gels. For the active system, this is not the case. To distinguish between thermal averages and averages over the non-equilibrium, motor-driven system we write the former averages as  $\langle \cdot \rangle$  and the latter ones as  $\langle \cdot \rangle_M$ .

To evaluate the power spectrum of the active gel we use the Greens function computed in the previous section and make the following assumptions regarding the force density  $\mathbf{f}^{(u)}$ . The stochastic force density acting on the network has two uncorrelated parts coming from motor-induced (non-equilibrium) forces and the usual thermal force associated with equilibrium statistical mechanics, i.e., those set by the fluctuation-dissipation theorem. Thus, we write

$$\mathbf{f}^{(u)} = \mathbf{f}_{\text{motor}}(\mathbf{x}, t) + \mathbf{f}_{\text{thermal}}(\mathbf{x}, t). \quad (23)$$

The thermal forces on the network  $\mathbf{f}_{\text{thermal}}(\mathbf{x}, t)$  are selected from the spatially uniform probability distribution. The same cannot be said for the motor-induced forces. The motor-induced forces come in correlated pairs. See Fig. 1 for a schematic illustration. The motor acts on a pair of parallel filaments to move one of them past other. The two filaments in question then exert a pair of equal and oppositely directed forces at the cross-links. Note that the motor-induced forces are directly inwardly towards the motor itself. The actin filaments can sustain large tensile stresses allowing the motor force pair to be transmitted significant distances through the network on the scale of the mean distance between cross-links. These same filaments, however, cannot sustain large compressive forces before undergoing an Euler buckling instability. Thus, the motors generate only an extended force dipole in the network. For a motor centered at the origin of the coordinate system the force density it generates has a spatial distribution of the form

$$\mathbf{f}_{\text{motor}}(\mathbf{x}, t) = f_0 \hat{\mathbf{a}} [\delta(\mathbf{x} + \mathbf{a}/2) - \delta(\mathbf{x} - \mathbf{a}/2)]. \quad (24)$$

The direction with the force pair  $\hat{\mathbf{a}}$  is also a random variable that is isotropically distributed since we assume that the filaments themselves are so distributed. The distribution of the magnitude of the force pair separation is presumably peaked at a scale comparable to the mean distance  $\ell_c$  between cross-links along a filament, which is larger than the mesh size of the network and less than the contour length of a filament. In Ref. [32], for instance, a distance  $\ell_c \sim 2.5 \mu\text{m}$  was inferred from the experiments.

We now focus on the temporal dependence of these motor-induced forces. The individual myosin motors that drive the network have a short duty cycle producing only transient kicks to the network. These motors, however, polymerize in solution to form aggregates of order  $10^2$  motors. The motor aggregates collectively generate forces on the scale of a few pN acting for on the order

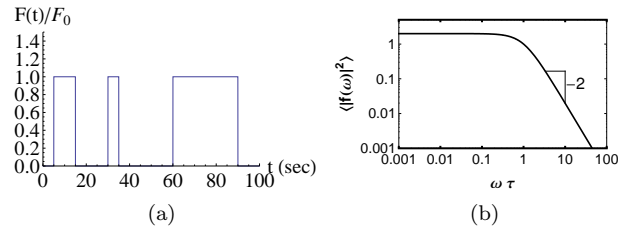


FIG. 5: (a) A representative example of a time series of motor forces from one myosin motor. The duration of the periods where the force takes the value  $F_0$  is selected from the probability distribution  $P(t)$  as discussed in the text. (b) The power spectrum of the motor forces. The angled brackets represent an average over  $P(t)$  and is not a thermal average.

of tens of seconds. These forces generically rise gradually from zero to their maximum and the drop back to zero abruptly when the aggregate detaches from its substrate, one or both of the two F-actin filaments to which it was bound. We will show that the rapid off kinetics injects a great deal of low frequency noise. To capture this effect we model the non-equilibrium motor forces as a series of square pulses of amplitude  $F_0 \approx 5pN$  and varying duration. A typical example is shown in Fig. 5a. Given that the probability per unit time of a motor detachment event from its substrate is independent of duration over which the motor has been active, it is reasonable to assume that the distribution of durations of motor activity  $T$  is Poisson distributed with mean  $\tau$

$$P(T) = \frac{1}{\tau} e^{-T/\tau}. \quad (25)$$

For the experiments in question  $\tau$  is on the order of tens of seconds.

Working in the frequency domain, a square pulse of force of duration  $T$  (as shown in Fig. 5a) generates a force spectrum in the frequency domain of

$$f(\omega; T) = \frac{2f_0 \sin(\omega T/2)}{\omega T}. \quad (26)$$

The instantaneous turn-off of the force is the source of the  $\omega^{-1}$  growth of force spectrum at small frequencies. We assume that the forces making up the time series as shown in Fig. 5a are mutually uncorrelated in time so that the temporally averaged motor-induced force fluctuation spectrum is given by

$$\langle |f(\omega)|^2 \rangle_M = \int_0^\infty dT \frac{1}{\tau} e^{-T/\tau} |f(\omega; T)|^2 = \frac{2f_0 \tau^2}{1 + (\tau \omega)^2}. \quad (27)$$

The spectrum of force fluctuations is Lorentzian as shown in Fig. 5b. We emphasize that the angled brackets in Eq. (27) represent an average over the distribution of on-times for the motors given by Eq. (25), and not a thermal average. The end of the plateau of the Lorentzian in the mean on-time  $\tau \sim 10\text{s}$  of the motors. At frequencies high

enough that  $\omega\tau > 1$ , the force power spectrum decays as  $\omega^{-2}$  at least out to frequencies comparable to inverse of the force decay time of an individual myosin motor. The available data on myosin-II suggests that this frequency is on the order of  $10^3\text{Hz}$  [69]. The thermal forces acting on the network generate white noise (assuming the network's shear modulus is not viscoelastic) of an amplitude proportional to the solvent viscosity and to the absolute temperature. This frequency-independent thermal noise, not shown here, eventually sets a noise floor for the system. The cross-over point to thermal noise dominance at high frequencies depends on overall amplitude of the motor-induced noise, which in turn depends on the density and activity of the ATP-consuming motors. In Fig. 5b this amplitude is set arbitrarily.

### III. RESULTS

#### A. The fluctuation spectrum

We now calculate the fluctuation spectrum of the non-thermal motor-driven strain field. We do this by setting thermal driving terms to zero and then averaging the displacement field at the origin of the coordinate system over the spatially and temporally varying motor fluctuations. This average is computed by integrating over the position of the center of force pair  $\mathbf{r}$ , and the separation vector between the two forces making up the force pair  $\mathbf{a}$ . Using the response function  $\alpha_{ij}(\mathbf{r}, \omega)$  computed above, we may write the strain fluctuation spectrum (evaluated at the origin) as

$$\langle |\mathbf{u}(\omega)|^2 \rangle_M = n \int d^3\mathbf{r} \int d^3\mathbf{a} \mathcal{P}_f(\mathbf{a}) |\mathbf{x}(\omega; \mathbf{r}, \mathbf{a})|^2, \quad (28)$$

where we define  $\mathbf{x}(\omega; \mathbf{r}, \mathbf{a})$  to be the amplitude of the displacement field at the origin and at frequency  $\omega$  in response to a motor-induced force pair of the form of Eq. (24), but centered at  $\mathbf{r}$ . The distributed dipole of forces is separated by the vector  $\mathbf{a}$ . Using the response function of the two-fluid model to a point force and superposition, this displacement is given by

$$|\mathbf{x}(\omega; \mathbf{r}, \mathbf{a})|^2 = \sum_{i=1}^3 \left[ \alpha_{ij}(-\mathbf{r} + \mathbf{a}/2, \omega) - \alpha_{ij}(-\mathbf{r} - \mathbf{a}/2, \omega) \right] f_0(\omega) \hat{a}_j \Big|^2. \quad (29)$$

In the above response function  $\alpha_{ij}$  is given by Eq. (18) and the temporal correlations in the motor force fluctuations are defined by Eq. (27); we work in the limit where  $\omega\tau \gg 1$ . We have implicitly assumed in Eq. (28) that the density  $n$  of active motors is uniform in space and in time. The distribution of separation vectors of force pairs

$$\mathcal{P}_f(\mathbf{a}) = \frac{1}{4\pi} p_f(|\mathbf{a}|) \quad (30)$$

is rotationally isotropic and strongly peaked at a length scale on the order of the mean distance between cross-links in the network. This distance is greater than the mesh size and less than a typical filament length. Note that in an isotropic elastic medium it is sufficient to integrate over all positions of the center of the force pair  $\mathbf{r}$  at a fixed orientation of that pair  $\hat{\mathbf{a}}$ . In the following we approximate this strongly peaked distribution in Eq. (30) by a delta function.

We compute the motor-driven strain fluctuation power spectrum for a semiflexible network having a frequency-dependent complex rheology given by a low frequency plateau modulus  $G(\omega) \simeq G_0$  and a high frequency  $G(\omega) \sim (-i\omega)^{3/4}$  regime for frequencies above some  $\omega_0$ , typically of order  $1\text{-}10\text{s}^{-1}$  [18, 70, 71]. We approximate this behavior by

$$G(\omega) \simeq G_0 \left[ 1 + \left( -i \frac{\omega}{\omega_0} \right)^{3/4} \right] \quad (31)$$

$$B(\omega) = 3G(\omega). \quad (32)$$

Using Eqs. (31), (32) in Eq. (28) and computing that

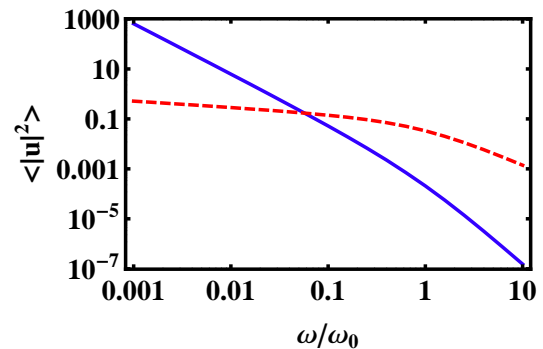


FIG. 6: (color online) The power spectral density of network strain fluctuations predicted for a motor-driven network (solid, blue) and for a network in thermal equilibrium (dashed, red). The vertical position of the motor-induced spectrum (solid, blue) depends on an arbitrarily set density of active motors. Both spectra as plotted against the dimensionless frequency  $\omega/\omega_0$  as described in the text.

integral numerically we plot (blue) the predicted fluctuation spectrum in Fig. 6 the power spectral density of the strain fluctuations of the network entirely due to the action of endogenous molecular motors. The fluctuation spectrum is shown as a function of the dimensionless frequency  $\omega/\omega_0$ . We note, however, that this is only an approximation. In particular, although this incorporates both the low frequency plateau and high-frequency stiffening of the network due to the dynamics of individual filaments, it does not accurately capture the imaginary part of the shear modulus in the plateau regime. Although this may invalidate the thermal spectrum at low frequencies, it does not significantly affect the active fluctuations that dominate at low frequency. Thus, this sim-

ple approximation in Eqs. (31), (32) illustrates an expected  $\langle |u|^2 \rangle \sim \omega^{-2}$  in the low-frequency plateau regime, where active stress fluctuations dominate [13, 15, 56], as well as a high-frequency regime dominated by thermal effects, in which  $\langle |u|^2 \rangle \sim \omega^{-7/4}$  is observed for equilibrium gels [18].

To examine how the shape of the motor-driven fluctuation spectrum differs from the equilibrium one, we compute the latter using the fluctuation-dissipation theorem. Specifically, we compute the mean squared fluctuations for the transverse and longitudinal parts of the strain field in thermal equilibrium using

$$\langle |u_T(\omega)|^2 \rangle \propto \frac{T}{\omega} \text{Im} \left[ \frac{1}{G(\omega)} \right] \quad (33)$$

$$\langle |u_L(\omega)|^2 \rangle \propto \frac{T}{\omega} \text{Im} \left[ \frac{1}{B(\omega)} \right]. \quad (34)$$

Here  $u_{T,L}(\omega)$  are the transverse (T) and longitudinal (L) parts of the strain field evaluated at frequency  $\omega$  and at one location in real space, i.e.  $\mathbf{x} = \mathbf{0}$ . In Eqs. (33), (34), we have implicitly assumed that the displacement of a tracer particle embedded in the material depends only on the strain field of the network; the effect of the solvent is only to make a correction to the effective viscoelastic moduli of the network:  $G(\omega)$  and  $B(\omega)$ . From our exploration of the transverse modes of the system, this is likely to be accurate there validating Eq. (33). The use of Eq. (34) is more suspect. This is especially true at high frequency, since  $B(\omega)$  should actually increase more rapidly with frequency within the two-fluid model than suggested by Eq. (32); i.e., the medium becomes strictly incompressible at high frequency, while it retains a finite shear modulus.

As in the case of the motor-driven fluctuations, the thermal fluctuation spectrum is translationally invariant; we suppress the positional degrees of freedom. The elastic moduli are taken from Eqs. (31), (32). Finally, the proportionality constants above are irrelevant as the overall scale of the motor-driven fluctuation spectrum is proportional to the number density of active motors, which is not independently known. Thus, we are free to shift the motor-induced fluctuation spectrum (blue line) vertically relative to the thermal fluctuation spectrum (red line). We note that expected fluctuation spectrum seen in active gel experiments will be the sum of the two curves shown in Fig. 6 since the expected force fluctuation spectrum is the incoherent or uncorrelated sum of the colored motor-induced noise and the white thermal noise.

In spite of this remaining freedom to shift the two curves relative to each other, we can make some unambiguous predictions based on the theory. The first is that motor-induced or non-thermal fluctuations will always dominate the spectrum at low enough frequencies while the thermal fluctuations of the material dominate at higher frequencies. The cross-over frequency between these two regimes depends on the density of ac-

tive motors, moving to higher frequencies as that density increases. Secondly we note that the normally seen low-frequency plateau typical of the thermal fluctuation spectrum of elastic solids disappears in the motor-driven system. At these low frequencies the fluctuation spectrum dominated by motor activity grows as  $1/\omega^2$ . This can be understood as follows: At these low frequencies the elastic moduli of the are essential frequency independent, i.e.  $G(\omega) \rightarrow \text{const}$ . The expected fluctuation spectrum then takes the form

$$\langle |u|^2 \rangle \sim \frac{\langle |f(\omega)|^2 \rangle_M}{|G(\omega)|^2} \sim \omega^{-2}, \quad (35)$$

since the motor-driven spectrum exhibits  $\omega^{-2}$  growth at low frequencies as long as  $\omega\tau > 1$  as seen from Eq. (27).

Transforming back to the time domain, Eq. (35) implies that the position of a tracer embedded in the active network  $x(t)$  appears to diffuse so that  $\langle |x(t) - x(0)|^2 \rangle \sim t$  at least for time scale smaller than  $\tau$ , the mean active time of the motors. Since this time scale can be on the order or tens of seconds, tracer particles fixed in an active gel or embedded cytoskeletal components such as microtubules, will appear to diffuse over typical experimental time scales even though the tracer is not actually moving through the network [13, 15, 56].

## B. The modulus in the active state

We can understand the dramatic increase in the modulus of the active network relative to the same system in thermal equilibrium as a simple application of the force extension relation of a worm-like chain in the limit that the filament length  $L$  is significantly smaller than the thermal persistence  $\ell_P$  of the chain [34]. In this limit the Hamiltonian for the transverse undulations  $\mathbf{t}(s)$  of a filament under tension  $f$  can be linearized as

$$H_{WLC} = \int_0^L ds \frac{1}{2} \left[ \kappa \left( \frac{d^2 \mathbf{t}}{ds^2} \right)^2 + f \left( \frac{d\mathbf{t}}{ds} \right)^2 \right], \quad (36)$$

where the bending modulus of the chain is given by  $\kappa = k_B T \ell_P$ . The vector field  $\mathbf{t}$  lies in the plane normal to the average direction of the filament and is parameterized by the arc length  $s$  on that filament. The total filament contour length is  $L$  so that  $0 < s < L$ . For the network to which we will apply this calculation, the contour length  $L$  refers to the mean distance between consecutive cross-links along a F-actin filament since the cross-links are expected to effectively pin the transverse undulations.

Working with this quadratic Hamiltonian and pinned boundary conditions, i.e.  $\mathbf{t}(0) = \mathbf{t}(L) = 0$ , one can calculate the length stored in these transverse undulations of the filament in thermal equilibrium at a given tension. This stored length  $\Delta L$  can be written as a sum over sinusoidal undulatory modes of the chain as

$$\Delta L = \frac{k_B T L^2}{\kappa \pi^2} \sum_{n=1}^{\infty} \frac{1}{n^2 + f/f_0}, \quad (37)$$

where  $f_0 = \frac{\kappa\pi^2}{L^2}$ . For F-actin filaments having a persistence length of  $17\mu\text{m}$  and a contour length on the order of microns, this tension scale is  $\approx 0.1\text{pN}$ . Applied tensile stresses larger than this value will significantly change the spectrum of transverse thermal undulations of the filament.

The remaining sum in Eq. (37) can be performed so we may write the thermal equilibrium value of the extension of the filament  $L_T$  as

$$\frac{L_T(f)}{L} = 1 - \frac{L}{\ell_P\pi^2}g\left(\frac{f}{f_0}\right), \quad (38)$$

where

$$g(x) = \frac{-1 + \pi x^{1/2} \coth[\pi x^{1/2}]}{2x}. \quad (39)$$

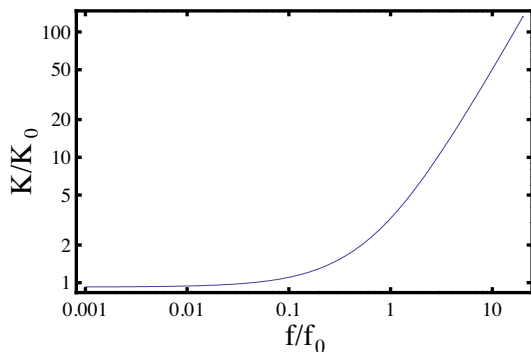


FIG. 7: The extensional modulus of a semiflexible actin filament normalized by its value in thermal equilibrium as a function of the non-dimensionalized applied tension  $f/f_0$ . The nonlinear stiffening of individual actin filaments under motor-induced tension can account for the overall increase of the network's modulus in response to motor activity.

From Eqs. (38), (39) we compute the effective extensional modulus

$$K = \frac{df}{dL} \quad (40)$$

by taking the inverse of the negative derivative of the stored length  $\Delta L$  from Eq. (37) with respect to the applied tension  $\sigma$ .

In Fig. 7 we plot the relative increase in the extensional modulus of an actin filament as a function of the non-dimensionalized applied tension  $f/f_0$ . The effective modulus at tension  $f$  is normalized by its linear value at vanishing small tension. Examining this curve we see that the modulus increases approximately non-linearly with tension, as  $K \sim f^{3/2}$  in the high-tension regime[23, 56], and that the effective modulus of the filaments increases about one hundred fold for  $f \approx 10f_0$ , which corresponds to tensions on the order of a few pN for network strands of length  $\ell_c \simeq 2\mu\text{m}$ . Noting that the effective modulus of the network is proportional to the product of  $K$ , the network density  $\rho_L$  (equal to filament length per unit volume), and the mean distance

between cross-links,  $\mu = \frac{1}{15}K\rho_L\ell_c$  [70, 71], we see that, under a mean tension of only a few pN, the network's modulus can increase by a factor of  $10^2$ . Such tensile forces of the magnitude expected to be produced by active myosin motors. Thus, the interaction of the inherent elastic nonlinearity of the semiflexible filaments making up the network and the motor-induced tensions is sufficient to account for the drastic stiffening of the out of equilibrium system.

#### IV. DISCUSSION

We have developed a driven two-fluid model of a semiflexible network driven out of equilibrium by molecular motors. In the limit of low active motor density, we compute the predicted fluctuation spectrum of the gel and find that it differs significantly from the typical microrheological results of such materials in thermal equilibrium.

In summary, we find a active-motor-density dependent enhancement of the low frequency noise in the strain field that generically dominates the tracer fluctuation spectrum at low frequencies. One of the consequences of this low frequency noise enhancement is that tracers will appear to diffuse in the network even when their size is much larger than the mesh size. At longer time scales the mean squared displacement of the tracers will plateau, exhibiting typical subdiffusive behavior, and both the time scale for this plateau and the particles' effective diffusion constant at shorter times will depend on the density of active motors. At high enough frequencies, the motor-induced fluctuations will always form a subdominant correction to the usual thermal fluctuations of the gel. The cross-over frequency between the small  $\omega$ , motor-dominated part of the spectrum and the large  $\omega$  thermally dominated part itself depends on the number density of active motors.

We also examined in a simple mean field approach that the interaction of the inherent elastic nonlinearity of the semiflexible filaments under tension with motor-induced forces leads to an approximately one hundred fold stiffening of the motor-driven network over the thermal one. Motor generated tensions on the order of one pN, if distributed evenly throughout the network, can lead to this dramatic change in the elastic properties of the system.

We conclude with a discussion of the limits of the theory and the extensions of this preliminary work that we intend to pursue. One of principal questions raised by the use of the two-fluid continuum model concerns its validity at short distances. This is of particular concern in the driven system since the molecular motor induced forces generate a type of distributed or finite size dipole of characteristic length equal to the separation between the two force centers  $\approx \ell_c$ , the mean distance between consecutive cross-links along a filament. In the application of the two-fluid model to *flexible gels* it is reasonable to take the mesh size  $\xi$  to be the short distance limit of the validity of the assumption of continuum elasticity.

For the case of interest  $\ell_c \approx 10\xi$ , so one might conclude that the two-fluid description is applicable to describe even the local displacement field around a distributed dipole. Cytoskeletal networks, however, are semiflexible; each filament has another inherent length scale, the thermal persistence length  $\ell_P$ , which for F-actin is on the order of  $20\mu\text{m}$ . Thus, for the system of interest we have  $\ell_P \approx 10\ell_c$  calling into question the application of continuum mechanics on the scale of the distributed force dipoles.

Recent work [72–75, 77, 78] has shown that semiflexible networks admit a new geometric/mechanical cross-over between an affine regime, well described by continuum mechanics down to length scales on the order of  $\ell_c$ , and a nonaffine regime where the network deformation cannot be described by continuum mechanics over mesoscopic lengths far greater than  $\ell_c$ . This cross-over is controlled primarily by filament cross-link density. In the affine regime the deformation around a point force can be described in terms of the continuum elastic solution down to the scale of  $\ell_c$ , suggesting that the short distance limit of the validity of the two-fluid model is at most marginally relevant to the theory presented here. In sparser networks, on the other hand, we expect to see significant deviations of the strain field around a point force over lengths much larger than  $\ell_c$  [76]. In the non-affine regime the two-fluid model is clearly inadequate to calculate network's response to motor forces. New ideas are required to explore such driven nonaffine systems.

In addition, both of the calculations presented above ignore the interaction of motors mediated by the strain field in the network. Such effects may become important at higher motor concentrations. The motor interactions are expected to take two forms. Our calculations have so far assumed that the effects of motors can be simply added. This will not be the case when the motors interact through the elastic nonlinearity of the semiflexible network. Such interactions should have measurable effects on the non-equilibrium strain fluctuations of the system when the density of active motors becomes sufficiently high.

To explore this point, consider the effect of two motors on the displacement of a tracer particle. If a motor is active in a particular region it will generate a contribution to the strain field (and thus to the displacement of nearby tracer particles using for microrheology) but also contribute to the local stiffening of the network. Should a second motor become active in same area, its contribution to the displacement of the tracer will be influenced by the local stiffening of the network due to the activity of the first motor. Since the motors generate fixed forces and not fixed displacements, the effect of the second motor on the displacement of the tracer will be diminished due to the increase of the network's effective modulus in response to the first motor's activity. Thus, the effects of multiple active motors will not be simply additive in the high motor concentration limit. Secondly, the forces generated by one motor in the network may

act to detach near-by motors from their substrate. It is well-known that the off-rate of non-covalent biochemical bonds is exponentially sensitive to applied load [79, 80]. Since the motors act as transient cross-linkers in the network, changes in the local stress state of the system will influence the off-rate of motors. In particular we expect that the activity of a motor will *decrease* the probability of the activity of near-by motors. This effect should lead to spatial anti-correlations in the density of active motors in the network. This effect should play a role as an  $n^2$  correction to the integral over motor-induced strain fluctuations leading to a type of viral expansion in the active motor density.

The stiffening of the network in response to motor activity will also depend on the density and spatial distribution of active motors. Our calculation shows that a typical value expected for the tension in an active network is sufficient to explain the two order of magnitude increase in its effective modulus. The calculation, however, does not address how this modulus quantitatively depends on the density of active motors. One might imagine that each active motor creates a volume around it in which the network's local modulus is effectively stiffened. The macroscopic stiffening of the network then results from a type of percolation of such stiffer regions occurring at a critical mean density of active motors. Based on this reasoning, one might expect the dependence of effective macroscopic modulus on active motor density to be highly nonlinear. This simple prediction is complicated by the fact that a low density of stiffer inclusions is known to effect the long length scale mechanics of an elastic solid. Such an effect has been studied in the context of carbon black reinforced rubbers.

### Acknowledgements

We thank D. Mizuno, C.F. Schmidt, and A. Lau for enlightening discussions. This work was supported in part by NSF (grant-CMMI-0800533) and FOM/NWO.

### Appendix A: The M matrix

The  $6 \times 6$  matrix is most easily understood in terms of a  $2 \times 2$  block matrix in which each block is a  $3 \times 3$  matrix whose indices run over the usual Cartesian space coordinates in three dimensions. In this form the matrix can be written in the Fourier domain in terms of wavevector  $\mathbf{k}$  and frequency  $\omega$  as

$$\mathcal{M}_{\alpha\beta} = \begin{pmatrix} A_{ij} & -\Gamma\delta_{ij} \\ i\omega\Gamma\mathcal{P}_{ij}^T(\mathbf{k}) & B_{ij} \end{pmatrix}. \quad (\text{A1})$$

We have defined the  $3 \times 3$  matrices to be

$$A_{ij} = -i\omega\Gamma\delta_{ij} + \mu k^2 \mathcal{P}_{ij}^T(\mathbf{k}) + Bk^2 \mathcal{P}_{ij}^L(\mathbf{k}) \quad (\text{A2})$$

$$B_{ij} = (-i\omega\rho + \eta k^2 + \Gamma) \delta_{ij} \quad (\text{A3})$$

so that  $\mathcal{M}_{\alpha\beta} = A_{\alpha\beta}$  for  $\alpha, \beta \leq 3$ . Similarly,  $\mathcal{M}_{\alpha\beta} = B_{\alpha-3, \beta-3}$  when both  $3 < \alpha \leq 6$  and  $3 < \beta \leq 6$  hold.

The equation of motion of the two-fluid system then can be written compactly as

$$\mathcal{M}_{\alpha\beta} \mathcal{U}_\beta = \mathcal{F}_\alpha, \quad (\text{A4})$$

where the 6-vector of the dynamical fields is given by

$$\mathcal{U}_\alpha = \begin{cases} u_\alpha & 1 \leq \alpha \leq 3 \\ v_{\alpha-3} & 4 \leq \alpha \leq 6 \end{cases} \quad (\text{A5})$$

In the above we suppress the  $\mathbf{k}$  and  $\omega$  dependence of this vector. The 6-vector of force densities driving these variables has a similar form:

$$\mathcal{F}_\alpha = \begin{cases} f^{(u)}_\alpha & 1 \leq \alpha \leq 3 \\ f_j^{(v)} \mathcal{P}_{\alpha-3, j}^\top(\mathbf{k}) & 4 \leq \alpha \leq 6 \end{cases} \quad (\text{A6})$$

where the sum on  $j$  runs over the three coordinates of the physical system and  $\mathbf{f}^{(u)}$ ,  $\mathbf{f}^{(v)}$  are the force densities driving the network and the fluid respectively. Looking at Eq. (A1) we note that the two off-diagonal blocks couple the dynamics of the displacement and fluid velocity fields; they are both necessarily proportional to  $\Gamma$ . In order solve for the response of the dynamical field  $\mathbf{u}$  and  $\mathbf{v}$  in terms of the applied force densities, it is necessary to invert the  $\mathcal{M}$  matrix. This is most naturally accomplished in the basis of longitudinal and transverse modes of the fluid and the network as can be seen from an examination of Eq. A2. The longitudinal part of the fluid velocity field decouples from the other dynamical variables. It is not driven due to the presence of the transverse projector in Eq. A6 and thus can be neglected.

### Appendix B: The longitudinal response tensor

In this appendix we transform the longitudinal response function from wave vector to position space. Doing this requires that we evaluate the integral

$$\mathcal{L}_{ij}(\mathbf{x}) = \int \frac{d^3 \mathbf{q}}{(2\pi)^3} e^{i\mathbf{q} \cdot \mathbf{x}} \frac{\hat{q}_i \hat{q}_j}{-i\omega\Gamma + Bq^2}. \quad (\text{B1})$$

Examining the structure of the integrand above it is clear that that

$$\mathcal{L}_{ij}(\mathbf{x}) = t_1 \delta_{ij} + t_2 \hat{x}_i \hat{x}_j. \quad (\text{B2})$$

To determine the remaining constants, we evaluate the trace of the tensor and the product  $\hat{x}_i \hat{x}_j \mathcal{M}_{ij}(\mathbf{x})$ . The trace of the tensor can be simply written as

$$\mathcal{L}_{ii}(\mathbf{x}) = \frac{1}{2\pi^2 |\mathbf{x}|} \int_0^\infty dq \frac{q \sin(q|\mathbf{x}|)}{-i\omega\Gamma + Bq^2}. \quad (\text{B3})$$

Nondimensionalizing the integral and we may write this as

$$\mathcal{L}_{ii}(\mathbf{x}) = \frac{1}{2\pi^2 B |\mathbf{x}|} \int_0^\infty ds \frac{s \sin(s)}{s^2 - ix^2/\ell^2(\omega)}, \quad (\text{B4})$$

where we have introduced the penetration length defined by Eq. (16) and repeated indices are summed over. Performing the remaining integral, we find that

$$\mathcal{L}_{ii}(\mathbf{x}) = \frac{1}{4\pi B r} e^{-\kappa r/\ell(\omega)}, \quad (\text{B5})$$

where  $r = |\mathbf{x}|$  and  $\kappa$  is the root of unit defined in Eq. (15). It is clear that in the static limit,  $\omega \rightarrow 0$ , the penetration length diverges for any elastic solid, i.e. a material where  $\lim_{\omega \rightarrow 0} B(\omega) = B_0 > 0$ , so that the above result simplifies to  $\mathcal{L}_{ii}(\mathbf{x}) = 1/(4\pi|\mathbf{x}|)$  as is expected for this part of the response function of an isotropic, elastic solid due to a point force at the origin.

To compute the scalar product,  $\hat{x}_i \hat{x}_j \mathcal{L}_{ij}(\mathbf{x}) = \mathcal{I}$ , we note this integral is actually simply related to that shown in Eq. (B4). In this case we find

$$\mathcal{I} = -\frac{1}{2\pi^2 B} \frac{\partial^2}{\partial x^2} |\mathbf{x}| \int_0^\infty ds \frac{\sin(s)}{s} \frac{1}{s^2 - ix^2/\ell^2(\omega)}. \quad (\text{B6})$$

Evaluating the remaining integral as above and taking the necessary derivatives we find that

$$\mathcal{I} = \frac{1}{4\pi B r} \left[ e^{-\kappa \frac{r}{\ell}} + \frac{2i\kappa\ell}{r} e^{-\kappa \frac{r}{\ell}} - \frac{2i\ell^2}{r^2} (1 - e^{-\kappa \frac{r}{\ell}}) \right] \quad (\text{B7})$$

From Eq. (B2)  $\mathcal{L}_{ii}(\mathbf{x}) = 3t_1 + t_2$  and  $\mathcal{I} = t_1 + t_2$ , so by using Eqs. (B5) and (B7) we may determine the two unknown functions making up the longitudinal response function. From these results and simple algebra we find that this response tensor takes the form given by Eq. (12).

It is important to check the static limit of these results. In the  $\omega \rightarrow 0$  limit, the solvent can play no role in generating stresses so the mechanics of the two-fluid system must simplify to that of an isotropic continuum elastic material. As seen in Eq. (B3), in the static limit  $\ell \rightarrow \infty$  so  $\mathcal{L}_{ii}(\mathbf{x}) \rightarrow 1/(4\pi B r) [1 - \kappa r/\ell]$ . It is simple to check that first term corresponds to the usual result for the elastic Green's function in an isotropic continuum. From Eq. (B7) it is clear that the  $r/\ell \rightarrow 0$  limit is somewhat nontrivial. Expanding the exponentials, one finds that  $\mathcal{I} \rightarrow 1/6\pi B r [0 + i\kappa r/\ell]$  so that this term vanishes in the static limit in agreement again with the results of continuum elasticity.

### Appendix C: The transverse response

The transverse part of the network's response to a point force applied at the origin and having a sinusoidal time dependence is given by

$$\mathcal{T}_{ij}(\mathbf{x}, \omega) = \int \frac{d^3 \mathbf{q}}{(2\pi)^3} \frac{e^{i\mathbf{q} \cdot \mathbf{x}} (-i\omega\rho_F + \Gamma + \eta q^2) (\delta_{ij} - \hat{q}_i \hat{q}_j)}{(-i\omega\rho_F + \Gamma + \eta q^2) (-i\omega\Gamma + \mu q^2) + i\omega\Gamma^2}. \quad (\text{C1})$$

This integral can be obtained by using Eq. (9) to extract the transverse response of the network to a force applied directly to it, i.e.  $\mathbf{f}^{(v)} = 0$ , and  $\mathbf{f}^{(u)} \sim \delta(\mathbf{x})e^{-i\omega t}$ . We simplify this expression by setting the solvent mass density to zero. The effect of going to this completely inertia free regime is that the transverse network and solvent waves now have an infinite propagation velocity. Based on our experience with the similarly inertia free Stokes equation (zero Reynolds number hydrodynamics) we expect the response of the system around a point force to decay as a power law in space and instantaneously update itself temporally so that the response is always in-phase with a sinusoidal drive at all points in space.

We also note that  $\Gamma q^2 \sim (\xi q)^2 \ll 1$  since the continuum model cannot remain valid at length scales comparable to the mesh size. Using these two simplifications we find that Eq. (C1) can be rewritten as

$$\mathcal{T}_{ij}(\mathbf{x}, \omega) \simeq \int \frac{d^3\mathbf{q}}{(2\pi)^3} e^{i\mathbf{q}\cdot\mathbf{x}} \frac{(\delta_{ij} - \hat{q}_i\hat{q}_j)}{(\mu - i\omega\eta)q^2}. \quad (\text{C2})$$

The physical meaning of this result is now more transparent. The term in the dominator is precisely that expected for inertia free elasticity theory for a system having a *viscoelastic* shear modulus  $G(\omega) = \mu - i\omega\eta$ . This shear response of the composite medium is simple the combination of the elastic response of the network ( $\mu$ ) and the viscous response of the solvent ( $-i\omega\eta$ ). Nothing in the above analysis precludes the consideration of a frequency-dependent viscoelastic modulus of the network itself:  $\mu \rightarrow \mu'(\omega) + i\mu''(\omega)$ . In fact we examine such a case in our final computation of the expected power spectrum of tracer motions.

Using the techniques employed in C, the remaining integral over wavevector can be performed yielding the result:

$$\mathcal{T}_{ij}(\mathbf{x}, \omega) = \frac{1}{8\pi|\mathbf{x}|(\mu - i\omega\eta)} [\delta_{ij} + \hat{x}_i\hat{x}_j]. \quad (\text{C3})$$

- 
- [1] T.D. Pollard and J.A. Cooper *Annul. Rev. Biochem.* **55**, 987 (1986).
- [2] P.A. Janmey *Curr. Opin. Cell Biol.* **3**, 4 (1991).
- [3] B. Alberts, D. Bray, J. Lewis, M. Raff, K. Roberts, and J.D. Watson, *Molecular Biology of the Cell* 3<sup>rd</sup> Ed. (Garland, New York, 1994).
- [4] D. Bray and J.G. White *Science* **239**, 883 (1988).
- [5] T.J. Mitchison and L.P. Cramer *Cell* **84**, 371 (1996).
- [6] M.-F. Carlier and D. Pantaloni, *J. Mol. Biol.* **269**, 459 (1997).
- [7] J.A. Cooper and D.A. Schafer, *Curr. Opin. Cell Biol.* **12**, 97 (2000).
- [8] N. Volkmann and D. Hanein *Curr. Opin. Cell Biol.* **12**, 26 (2000).
- [9] P. Bursac, G. Lenormand, B. Fabry, M. Oliver, D.A. Weitz, V. Viasnoff, J. P. Bulter, and J.J. Fredberg *Nat. Mat.* **4**, 557 (2005).
- [10] E. Paluch, C. Sykes, J. Prost, and M. Bornens, *Trend Cell Biol.* **16**, 5 (2006).
- [11] P. Bursac, B. Fabry, X. Trepate, G. Lenormand, J. P. Bulter, N. Wang, J.J. Fredberg, and S.S. An, *Biochem. Biophys. Res. Commun.* **355**, 324 (2007).
- [12] G. Lenormand, J. Chopin, P. Bursac, J.J. Fredberg, and J.P. Butler *Biochem. Biophys. Res. Commun.* **360**, 797 (2007).
- [13] A.C. Lau, B.D. Hoffman, A. Davies, J.C. Crocker, and T.C. Lubensky, *Phys. Rev. Lett.* **91**, 198101 (2003).
- [14] L. Deng, X. Trepate, J.P. Butler, E. Millet, K.G. Morgan, D.A. Weitz, and J.J. Fredberg, *Nature Materials* **5**, 636 (2006).
- [15] C.P. Brangwynne, F.C. MacKintosh, and D.A. Weitz, *Proc. Natl. Acad. Sci. USA*, **104**, 16128 (2007).
- [16] P.A. Janmey, S. Hvidt, J. Kas, D. Lerche, A. Maggs, E. Sachmann, M. Schliwa, and T.P. Stossel *J. Biol. Chem.* **269**, 32503 (1994).
- [17] J. Käs, H. Strey, J.X. Tang, D. Finger, R. Ezzell, E. Sachmann, and P.A. Janmey, *Biophys. J.* **70**, 609 (1996).
- [18] F. Gittes, B. Schnurr, P.D. Olmsted, F.C. MacKintosh, and C.F. Schmidt, *Phys. Rev. Lett.* **79**, 3286 (1997).
- [19] F.C. MacKintosh and P.A. Janmey, *Current Opinion in Solid State and Material Science* **2**, 350 (1997).
- [20] T. Gisler and D.A. Weitz *Phys. Rev. Lett.* **82**, 1606 (1999).
- [21] T.G. Mason, T. Gisler, K. Kroy, E. Frey, D.A. Weitz, *J. Rheol.* **44**, 917 (2000).
- [22] M. L. Gardel, M.T. Valentine, J.C. Crocker, A.R. Bausch, and D.A. Weitz *Phys. Rev. Lett.* **91**, 158302 (2003).
- [23] M.L. Gardel, J.H. Shin, F.C. MacKintosh, L. Mahadevan, P. Matsudaira, and D.A. Weitz *Science* **304**, 1301 (2004).
- [24] M.L. Gardel, J.H. Shin, F.C. MacKintosh, L. Mahadevan, P.A. Matsudaira, and D.A. Weitz *Phys. Rev. Lett.* **93**, 188102 (2004).
- [25] R. Tharmann, M.M.A.E. Clasesens, and A. R. Bausch *Biophys. J.* **90**, 2622 (2006).
- [26] B. Wagner, R. Tharmann, I. Hasse, M. Fischer, and A.R. Bausch *Proc. Natl. Acad. Sci* **103**, 13974 (2006).
- [27] A.R. Bausch and K. Kroy, *Nat. Phys.* **2**, 231 (2006).
- [28] J. Liu, G.H. Koenderink, K. E. Kaszo, F.C. MacKintosh, and D.A. Weitz *Phys. Rev. Lett.* **98**, 198304 (2007).
- [29] Y. Luan, O. Lieleg, B. Wagner, and A.R. Bausch *Biophys. J.* **94**, 688 (2008).
- [30] L. Le Goff, F. Amblard, and E.M. Furst *Phys. Rev. Lett.* **88**, 018101 (2001).
- [31] D. Humphrey, C. Duggan, D. Saha, D. Smith, J. Käs, *Nature* **416**, 413 (2002).
- [32] D. Mizuno, C. Tardin, C.F. Schmidt, and F.C. MacKintosh, *Science* **315**, 370 (2007).
- [33] P.M. Bendix, G.H. Koenderink, D. Cuvelier, Z. Dogic, B.N. Koeleman, W.M. Briehner, C.M. Field, L. Mahadevan, and D.A. Weitz, *Biophys. J.* **94**, 3126 (2008).
- [34] F.C. MacKintosh, J. Kas, and P.A. Janmey, *Phys. Rev. Lett.* **75**, 4425 (1995).
- [35] R. Aditi Simha and S. Ramaswamy, *Phys. Rev. Lett.* **89**, 058101 (2002).
- [36] Y. Hatwalne, S. Ramaswamy, M. Rao, and R. Aditi Simha, *Phys. Rev. Lett.* **92**, 118101 (2004).

- [37] S. Mishra and S. Ramaswamy, Phys. Rev. Lett. **97**, 090602 (2006).
- [38] D.T. Chen, A.W.C. Lau, C. A. Hough, M.F. Islam, M. Goulian, T.C. Lubensky, and A.G. Yodh, Phys. Rev. Lett. **99**, 148302 (2007).
- [39] T.G. Mason and D.A. Weitz, Phys. Rev. Lett. **74**, 1250 (1995).
- [40] F.C. MacKintosh and C.F. Schmidt, Curr. Opin. Coll. Interf. Sci. **4**, 300 (1999).
- [41] A.J. Levine and T.C. Lubensky Phys. Rev. Lett. **85**, 1774 (2000).
- [42] A.J. Levine and T.C. Lubensky Phys. Rev. E **63**, 041510 (2001).
- [43] R.T. Chen, E.R. Weeks, J.C. Crocker, M.F. Islam, R. Vrena, A.J. Levine, T.C. Lubensky, and A.G. Yodh Phys. Rev. Lett. **90**, 108301 (2003).
- [44] B. Fabry, G.N. Maksym, J.P. Butler, M. Glogauer, D. Navajas, and J.J. Fredberg, Phys. Rev. Lett. **87**, 148102 (2001).
- [45] C. Wilhelm, F. Gazeau, J.C. Bacri, Phys. Rev E **67**, 061908 (2003).
- [46] L. Limozin, A. Roth, and E. Sackmann, Phys. Rev. Lett. **95**, 178101 (2005).
- [47] B.R. Daniels, B.C. Masi, and D. Wirtz, Biophys. J. **90**, 4712 (2006).
- [48] M. Ballard, N. Despart, D. Icard, S. Féréol, A. Asnacios, J. Browaeys, S. Hénon, and F. Gallet, Phys. Rev E **74**, 021911 (2006).
- [49] Y.-L. Wang and D. Discher *Cell Mechanics* (Elsevier, Amsterdam, 2007).
- [50] S.S. Rogers, T.A. Waigh, and J.R. Lu, Biophys. J. **94**, 3313 (2008).
- [51] T.B. Liverpool and M.C. Marchetti, Phys. Rev. Lett. **90**, 138102 (2003).
- [52] K. Kruse, J.-F. Joanny, F. Jülicher, J. Prost, and K. Sekimoto, EPJE **16**, 5 (2005).
- [53] T.B. Liverpool and M.C. Marchetti, Europhys. Lett. **69**, 846 (2005).
- [54] M.E. Cates, S.M. Fielding, D. Marenduzzo, E. Orlandi, and J.M. Yeomans, Phys. Rev. Lett. **101**, 068102 (2008).
- [55] A.C. Callen-Jones, J.-F. Joanny, and J. Prost, Phys. Rev. Lett. **100**, 258106 (2008).
- [56] F.C. MacKintosh and A.J. Levine Phys. Rev. Lett. **100**, 018104 (2008).
- [57] P.-G. DeGennes, Macromol. **9**, 587 (1976).
- [58] P.-G. DeGennes, Macromol. **9**, 594 (1976).
- [59] F. Brochard and P.-G. deGennes, Macromol. **10**, 1157 (1977).
- [60] F. Brochard J. Phys. (Paris) **44**, 39 (1983).
- [61] M. Doi, in *Dynamics and Patterns in Complex Fluids: New Aspects of Physics and Chemistry* eds. A. Onuki and K. Kawasaki (Springer, Berlin, 1990).
- [62] A. Onuki, J. Phys. Soc. Jpn. **59**, 3423 (1990).
- [63] S.T. Milner, Phys. Rev. Lett. **66**, 1477 (1991).
- [64] B. Schnurr, F. Gittes, F.C. MacKintosh, and C.F. Schmidt, Macromol. **30**, 7781 (1997).
- [65] A.J. Levine and T.C. Lubensky, Phys. Rev. E **63**, 041510 (2001).
- [66] L.D. Landau and E.M. Lifshitz, *Theory of Elasticity* (Pergamon, Oxford, 1959).
- [67] P.C. Martin, O. Parodi, and P.S. Pershan, Phys. Rev. A **6**, 2401 (1972).
- [68] P.M. Chaikin and T.C. Lubensky *Principles of Condensed Matter Physics* (Cambridge University Press, Cambridge, 1995).
- [69] J. Howard *Mechanics of Motor Proteins and the Cytoskeleton* (Sinauer Associates Incorporated, 2001).
- [70] D.C. Morse, Macromol. **31**, 7044 (1998).
- [71] F. Gittes and F.C. MacKintosh Phys. Rev E **58** R1241 (1998).
- [72] D.A. Head, A.J. Levine, and F.C. MacKintosh, Phys. Rev. Lett. **91**, 108102 (2003).
- [73] J. Willhelm and E. Frey, Phys. Rev. Lett. **91**, 108103 (2003).
- [74] D.A. Head, A.J. Levine, and F.C. MacKintosh, Phys. Rev. E **68**, 061907 (2003).
- [75] D.A. Head, F.C. MacKintosh, and A.J. Levine, Phys. Rev. E **68**, 025101 (R) (2003).
- [76] D.A. Head, A.J. Levine, and F.C. MacKintosh, Phys. Rev. E **72**, 061914 (2005).
- [77] C. Heussinger and E. Frey, EPJE **24**, 47 (2007).
- [78] S. Roy and H.J. Qi, Phys. Rev E **77**, 061916 (2008).
- [79] G.I. Bell Science **200**, 618 (1978).
- [80] E. Evans and K. Richie, Biophys. J. **72**, 1541 (1997).